

Structural stability and magnetic properties of disordered $SmCo_{7-x}M_x$ (M=metal) modulated by valence electron structure

Wei Liu(刘葳), Yongquan Guo(郭永权), Boyang Li(李博洋), Yu Yao(姚羽), Haitao Kong(孔海涛), and Yichen Feng(冯奕晨)

Citation: Chin. Phys. B, 2026, 35 (**5**): 056104. DOI: 10.1088/1674-1056/ae1729
http://cpb.iphy.ac.cn; http://iopscience.iop.org/cpb

What follows is a list of articles you may be interested in

Structural stability and mechanical properties of Ni_xMo_yN ternary nitrides under high pressure: A first-principles study

Tao Wang(王涛), Ming-Hong Wen(温铭洪), Kai-Xuan Wang(王凯璇), Jia-Mei Liu(刘佳美), Wei-Hua Wang(王伟华), Xu-Ying Wang(王旭颖), and Pei-Fang Li(李培芳)

Chin. Phys. B, 2026, 35 (**3**): 036102. DOI: 10.1088/1674-1056/ae306f

High-entropy alloys in synergistic electrocatalytic conversion applications

Hui Zhang(张辉), Zhengxiong Liu(刘争雄), Le Fang(方乐), Yin Wang(王音), Shuai Chen(陈帅), and Wei Ren(任伟)

Chin. Phys. B, 2025, 34 (**8**): 086109. DOI: 10.1088/1674-1056/ade8e6

Morphology-tuned phase transition of MnO_2 nanorods under high pressure

Xue-Ting Zhang(张雪婷), Chen-Yi Li(李晨一), Hui Tian(田辉), Xin-Yue Wang(王心悦), Zong-Lun Li(李宗伦), and Quan-Jun Li(李全军)

Chin. Phys. B, 2025, 34 (**6**): 066105. DOI: 10.1088/1674-1056/adc192

Layer-dependent structural stability and electronic properties of $CrPS_4$ under high pressure

Jian Zhu(朱健), Dengman Feng(冯登满), Liangyu Wang(王亮予), Liang Li(李亮), Fangfei Li(李芳菲), Qiang Zhou(周强), and Yalan Yan(闫雅兰)

Chin. Phys. B, 2025, 34 (**6**): 066102. DOI: 10.1088/1674-1056/adc65f

Valence electron structures dependences of structural stability and properties of REX_3(RE=rare earth; X=In, Tl) and $RE(In, Co)_3$ alloys

Boyang Li(李博洋), Yongquan Guo(郭永权), Yi-Chen Feng(冯奕晨), Xinze Wang(王鑫泽), and Wei Liu(刘葳)

Chin. Phys. B, 2024, 33 (**11**): 116102. DOI: 10.1088/1674-1056/ad7575

Structural stability and magnetic properties of disordered $SmCo_{7-x}M_x$ (M = metal) modulated by valence electron structure

Wei Liu(刘葳), Yongquan Guo(郭永权)†, Boyang Li(李博洋),
Yu Yao(姚羽), Haitao Kong(孔海涛), and Yichen Feng(冯奕晨)

School of Energy Power and Mechanical Engineering, North China Electric Power University, Beijing 102206, *China*

(Received 26 August 2025; revised manuscript received 8 October 2025; accepted manuscript online 24 October 2025)

$SmCo_{7-x}M_x$ (M = Cu, Zr, Hf, Si, Ga) intermetallic compounds, with distinctive disordered crystal structure and excellent magnetic performance, are of great importance for application as high-temperature rare-earth permanent magnets. In this study, the relationship between the valence electronic structure, structural stability and magnetic and thermal properties of Sm(Co, M)$_7$ intermetallic compounds is revealed by using an empirical electron theory of solids and molecules. The structural stability is strongly related to the valence electronic structure that is modulated by doping the third element M into $SmCo_7$. The calculated bond lengths, magnetic moments and Curie temperatures show good agreement with experimental ones. The magnetic moment and Curie temperature strongly depend on the number of 3d magnetic electrons, and can be modulated by mutual electron transformation between 3d magnetic electron and covalence electron.

Keywords: Sm(Co, M)$_7$ pseudo-binary intermetallics, valence electron structure, structural stability, magnetic property

PACS: 61.50.Lt, 75.50.–y, 78.40.Kc, 31.10.+z

DOI: 10.1088/1674-1056/ae1729 **CSTR:** 32038.14.CPB.ae1729

1. Introduction

The Sm–Co 1:7 type intermetallic compound exhibits exceptional magnetic properties such as large coercivity and a high Curie temperature,[1–3] and its coercivity is similar to the $SmCo_5$ one formed by a nucleation mechanism.[4,5] The Sm–Co 1:7 phase is a metastable phase at high temperature,[6] and can be stabilized by doping a third element M (such as M = Zr, Cu, Hf, Si or Ga) into $SmCo_7$ at room temperature.[7–12] These pseudo-binary Sm(Co, M)$_7$ intermetallic compounds show excellent high-temperature magnetic properties and have potential application as high-temperature rare-earth permanent magnetic materials.[13–15] The Sm–Co 1:7 intermetallic has a $TbCu_7$-type structure, as shown in Fig. 1, where Co–Co dumbbell pairs randomly occupy the 2e crystal positions, regarded as a displacement from the Sm site (1a position) along the c-axis induced by substitution of a Co–Co pair for Sm with a replacement rate of 2/9; the other Co atoms fully occupy the 2c and 3g crystal sites.[16–18]

Theoretical studies of the structural stability and magnetic properties of Sm(Co, M)$_7$ intermetallic compounds are very limited due to the complicated atomic occupations. The spin-polarized MS-Xα method, which is a semi-empirical theory based on first principles, is used to study electronic orbital hybridization between Sm and Co atoms and magnetic stability of Sm(Co, M)$_7$ intermetallic compounds to reveal their magnetism.[19–21] The calculated lattice parameters and the preferred atomic occupations of the disordered Sm(Co, M)$_7$ intermetallic compound are in good agreement with the experimental ones.[19,20] In addition, the effects of doping on the magnetic properties of Sm(Co, M)$_5$ and Sm_2(Co, M)$_{17}$ (M = Cu, Ti, Zr, Hf, Mn, Cr) intermetallic compounds are studied by density functional theory (DFT),[21,22] which reveals the strong relation between their electronic structures and physical properties. However, the first-principles DFT approach is built in reciprocal space and is computationally intensive and time-consuming for calculations of energy-band structures and physical properties because it involves extensive complex calculus and mathematical-physics equations. An empirical electron theory of solids and molecules (EET) differs from the first-principles model in that it does not need complex electron density functions. EET[23] is built in real space and is based on Pauling's valence bond theory and Hume-Rothery's electron concentration theory. EET provides a method to explore the correlation between physical properties and valence electron structures. The physical properties in EET are modeled based on the distribution of electrons in the s, p, and d orbitals of atomic shells, lattice electrons in lattice spaces and near neighbor bond lengths. EET can calculate multiple physical properties simultaneously, including mechanical properties,[24] thermal properties,[25] magnetic properties,[26–29] light absorption band gap,[30] open-gate voltage in batteries[31,32] and physical properties of high-entropy alloys.[33,34] The calculated values of properties not only match the experimental ones well but also can even predict unmeasured values. In this study, the empirical electron theory of solids and molecules is used to systematically study the valence electron structure, structural

†Corresponding author. E-mail: yqguo@ncepu.edu.cn

© 2026 Chinese Physical Society and IOP Publishing Ltd. All rights, including for text and data mining, AI training, and similar technologies, are reserved.

stability, magnetic moment and Curie temperature of Sm–Co 1:7-type intermetallic compounds to reveal the physical mechanisms of their structural stability and magnetic properties.

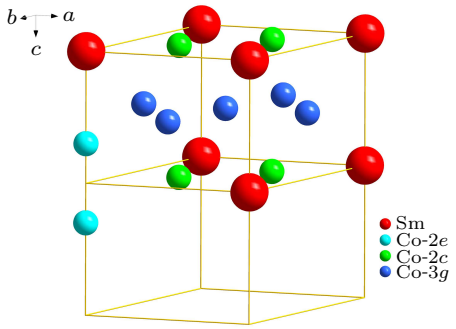


Fig. 1. Crystal structure of $SmCo_7$ phase.

2. Empirical electron theory of solids and molecules

EET mainly includes three basic hypotheses[35] and the bond length difference (BLD) method.[23,36]

Hypothesis 1 The atomic state in solids and molecules is a hybridization of two atomic states, called the ground state (h state) and the excited state (t state), respectively. Both states have valence electrons occupying s, p and d orbits for bonding with other atoms, lattice electrons for conducting electricity, 3d magnetic electrons for forming magnetic moments and dumb-pair electrons in the inner d shell for condensing the atomic radius. Meanwhile, a single-bond radius $R(l)$ is introduced to describe the change of distance between the peak position of charge density of the atomic orbit and the atomic nucleus.[31]

Hypothesis 2 The intermediate hybrid state between the two states is assumed to be quantized, and can be directly obtained by the sum of the weighed compositions of the two states based on a K-equation;[24] thus, all the hybrid data, including the numbers of various electrons and single-bond radii, are available in a so-called hybrid table for every element.[31]

Hypothesis 3 According to Pauling's bond length theory, the bond length $D_{uv}(n_\alpha)$ between u atoms and v atoms follows

$$D_{uv}(n_\alpha) = R_u(l) + R_v(l) - \beta \lg n_\alpha \quad (\alpha = A, B, \ldots, N), \quad (1)$$

where $R_u(l)$ and $R_v(l)$ are the single-bond radii for u and v atoms and n_α denotes the number of covalent electrons pairs on the αth bond. The parameter β represents the ability of electron clouds of bonding atoms to overlap; it is modified as

$$\beta = \begin{cases} 0.710, & n_\alpha^M < 0.250 \text{ or } n_\alpha^M > 0.750, \\ 0.600, & 0.300 \le n_\alpha^M \le 0.700, \\ 0.710 - 2.2\varepsilon, & n_\alpha^M = 0.250 + \varepsilon \text{ or } n_\alpha^M = 0.750 - \varepsilon, \end{cases} \quad (2)$$

where n_α^M represents the maximum value of n_α. The parameter β corresponds to 0.71 under the condition $n_\alpha^M < 0.25$ or $n_\alpha^M > 0.75$, and 0.6 when $0.30 \le n_\alpha^M \le 0.70$. In the calculation, the calculated numbers of covalent electron pairs are reordered in descending order. The maximum value of n_α is conventionally denoted by n_A. However, if the maximum number of covalent electron pairs fulfils the condition $n_\alpha^M \in [0.25, 0.30]$ or $n_\alpha^M \in [0.70, 0.75]$ a parameter ε is induced to estimate the difference of the calculated n_A from a reference value of either 0.75 or 0.25, i.e., ε equals $n_\alpha^M - 0.25$ when $n_\alpha^M \in [0.25, 0.30]$ or $0.75 - n_\alpha^M$ when $n_\alpha^M \in [0.70, 0.75]$, respectively. The parameter $\beta = 0.710 - 2.2\varepsilon$ in a constrained condition of $0 < \varepsilon < 0.05$.

The BLD method is used to determine the valence electron structures of all elements in $SmCo_{7-x}M_x$ by solving n kinds of theoretical bond lengths with the bond equations, as listed in Hypothesis 3.

For the first bond,

$$D_{uv}(n_A) = R_u(l) + R_v(l) - \beta \lg n_A. \quad (3)$$

For the ith bond,

$$D_{uv}(n_{\alpha i}) = R_{ui}(l) + R_{vi}(l) - \beta \lg n_{\alpha i}. \quad (4)$$

Then, we have

$$\Delta D_i = \Delta R_i - \beta \lg \gamma_i, \quad (5)$$

where $\Delta D_i = D_{uv}(n_A) - D_{uv}(n_{\alpha i})$, $\Delta R_i = R_u(l) + R_v(l) - R_{ui}(l) - R_{vi}(l)$ and $\gamma_i = n_{\alpha i}/n_A$.

Thus, we have

$$\gamma_i = \frac{n_{\alpha i}}{n_A} = 10^{\Delta R_i - \Delta D_i/\beta}.$$

The total number of covalence electrons n_c can be estimated by the sum of covalence electrons in all equivalent bonds,

$$n_c = \sum_i^n n_{ci}. \quad (6)$$

Then, we have

$$n_c = \sum_{\alpha=A}^{N} n_{\alpha i} I_\alpha = n_A \sum_{\alpha=A}^{N} \gamma_\alpha I_\alpha, \quad (7)$$

$$n_A = \frac{\sum_i^n n_{ci}}{\sum_{\alpha=A}^{N} \gamma_\alpha I_\alpha}, \quad (8)$$

$$n_\alpha = \gamma_\alpha n_A. \quad (9)$$

Thus, the theoretical length $\bar{D}_{uv}(n_\alpha)$ can be calculated by

$$\bar{D}_{uv}(n_\alpha) = R_u(l) + R_V(l) - \beta \lg n_\alpha \quad (\alpha = A, B, \ldots, N). \quad (10)$$

The hybrid states with various numbers of electrons for all elements can be determined by a criterion of bond length difference between the experimental and calculated bond lengths ΔD of less than 0.05 Å under the first-order approximation.

However, it is necessary to use an extra physical property criterion, which might be the melting point, the cohesive energy or the magnetic moment, to check the accuracy of valence electron structures with a maximum relative difference of 10% between the theoretical and experimental ones. According to the accurate valence electron structures, the other properties can be predicted, even the unmeasured ones. Detailed information about the three hypotheses and the BLD method is presented in the supporting information.

2.1. Models of cohesive energy and melting point

The cohesive energy of intermetallic compounds includes the bonding energy, electric potential, magnetic potential, condensing energy and residual energy caused by the electronegativity difference of bonding atoms:[32]

$$E_{\mathrm{C}} = \sum_{\alpha} \frac{b_\alpha I_\alpha n_\alpha}{\overline{D}_\alpha} f_\alpha + \frac{\sum b_{\mathrm{l}} n_{\mathrm{l}}}{\overline{D}} f' + \sum_i b_i a m^{3\mathrm{d}} - \sum_i b_i C_i W_i - |x\chi_{\mathrm{A}} - y\chi_{\mathrm{B}}|. \tag{11}$$

The melting point is modeled based on breaking of the strongest bond by heat vibration energy. It is assumed that the crystal structure is stabilized by the highest bonding energy. Thus, the highest bonding energy U_{B} is

$$U_{\mathrm{B}} = \frac{b_{\mathrm{A}} n_{\mathrm{A}}}{\overline{D}_{\mathrm{A}}} f_{\mathrm{A}} + b_{\mathrm{l}} \frac{n_{\mathrm{l}}}{I^\sigma \overline{D}} f' - \frac{\sum b_i C_i W_i}{I^\sigma} - \frac{\left| x E_n^{\mathrm{A}} - y E_n^{\mathrm{B}} \right|}{I^\sigma}. \tag{12}$$

At the critical temperature (melting point), the strongest bond is broken by the vibration of the thermal phonon, and other weak bonds are sure to be broken; the vibrating energy of thermal phonon should be equal to the bonding energy of the strongest bond. Thus, the energy of N mol of phonons is

$$U_{\mathrm{P}} = \frac{3}{2} NKT. \tag{13}$$

When $U_{\mathrm{B}} = U_{\mathrm{P}}$, we have

$$T_{\mathrm{m}} = \frac{\frac{b_{\mathrm{A}} n_{\mathrm{A}}}{\overline{D}_{\mathrm{A}}} f_{\mathrm{A}} + b_{\mathrm{l}} \frac{n_{\mathrm{l}}}{I^\sigma \overline{D}} f' - \frac{\sum b_i C_i W_i}{I^\sigma} - \frac{\left| x E_n^{\mathrm{A}} - y E_n^{\mathrm{B}} \right|}{I^\sigma}}{\frac{3}{2} NR}. \tag{14}$$

Detailed information on the models of cohesive energy and melting point is given in the supporting information.

2.2. Models of magnetic moment and Curie temperature

The magnetic moment originates from the 3d magnetic electrons of Co atoms; meanwhile, the rare earth Sm also contributes to the total magnetic moment of Sm(Co, M)$_7$. Thus, the theoretical magnetic moment ($\overline{M}_{\mathrm{S}}$) of Sm(Co, M)$_7$ is the sum of 3d electron numbers and the 4f effective potential of Sm with a trivalent state. The Curie temperature is modeled based on an assumption of melting of the ordered ferromagnetic structure by the thermal vibration energy, which is attributed to the increase in vibration energy of thermal phonons as the temperature increases. At the critical temperature, i.e., the Curie temperature (T_{c}), the vibration energy of the thermal phonons is just equal to the magnetic energy and enough to break the ordered magnetic structure. Since Sm contributes weakly to the magnetic moment at high temperatures, and the doping element M is non-magnetic, the Co–Co exchange interaction plays an important role in the magnetic performance of Sm(Co, M)$_7$ at high temperatures. Therefore, the magnetic energy per Co atom is

$$U_{\mathrm{m}} = g \frac{a \overline{m}_{\mathrm{Sm(Co},M)_7}}{\sum I_\alpha \gamma_{\alpha_{\mathrm{Co-Co}}}}. \tag{15}$$

When $U_{\mathrm{P}} = U_{\mathrm{m}}$, we have

$$T_{\mathrm{c}} = \frac{a}{\frac{3}{2}R} \frac{g \overline{m}_{\mathrm{Sm(Co},M)_7}}{\sum I_\alpha \gamma_{\alpha_{\mathrm{Co-Co}}}}. \tag{16}$$

Detailed information on the models is given in the supporting information.

3. Result and discussion

3.1. Structural stability and valence electron structure

The experimental bond lengths of Sm(Co, M)$_7$ are measured with Diamond software based on their crystallographic data. The calculated bond lengths match the experimental ones, with ΔD ranging from 0.01789 Å to 0.04990 Å, as shown in Tables S1 and S2 in the supporting information. Although the binary $SmCo_7$ phase does not exist naturally, its valence electron structure and physical properties have been successfully simulated through the application of EET. It has been suggested that the structural stability of Sm(Co, M)$_7$ strongly depends on three critical parameters — covalent electron number n_{c}, bonding factor f and shielding factor b_{l}[33] — and their correlations are shown in Fig. 2. This reveals that $SmCo_7$ can be stabilized by large numbers of covalence electrons n_{c} and a strong bonding factor f induced by introduction of M into $SmCo_7$. The $SmCo_6Ga$ intermetallic shows an abnormal phenomenon compared with unstable $SmCo_7$. Its n_{c} (26.057) is slightly less than that of $SmCo_7$ (26.989), but its bonding factor f (2.4391) and shielding factor b_{l} (121.71 kJ·Å/mol) are much higher than those of unstable $SmCo_7$ (f = 1.3095, b_{l} = 115.41 kJ·Å/mol), which can compensate for the slight reduction in n_{c}; thus $SmCo_6Ga$ can be stabilized.

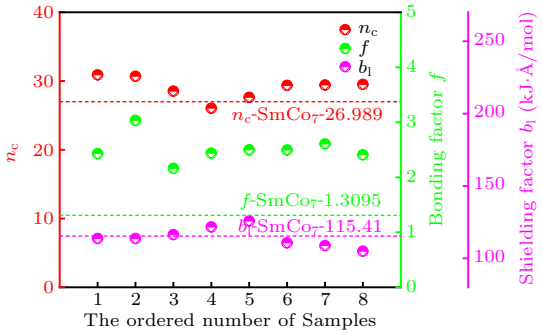


Fig. 2. The number of covalence electrons n_{c}, bonding ability f and shielding ability b_{l} for unstable $SmCo_7$ and Sm(Co, M)$_7$. 1, $SmCo_{6.9}Hf_{0.1}$; 2, $SmCo_{6.9}Zr_{0.1}$; 3, $SmCo_{6.1}Si_{0.9}$: 4, $SmCo_6Ga$; 5, $SmCo_{5.7}Ga_{1.3}$: 6, $SmCo_{6.2}Cu_{0.8}$; 7, $SmCo_{5.5}Cu_{1.5}$; 8, $SmCo_4Cu_3$.

The effects of various electrons on the structural stability of Sm(Co, M)$_7$ are shown in Fig. 3. The number of valence electrons n_d shows an inverse correlation with the number of lattice electrons n_l, as shown in Fig. 3(a). This is attributed to the mutual electronic transformations between valence electrons on the d orbit and lattice electrons on the s orbit by d–s or s–d hybridization. Such electron transitions modulate the number of covalence electrons and the structural stability. Magnetic electrons can also modulate the number of covalence electrons by mutual electron transformations between valence electrons and 3d magnetic electrons on the 3d orbital of Co atoms at 2e and 3g sites, as shown in Fig. 3(b). A balance is made between structural stability and magnetic properties by modulating the number of covalence electrons n_c (to stabilize the Sm(Co, M)$_7$ structure) and the number of 3d magnetic electrons (to improve the magnetic properties). The bonding factor f depends upon the numbers of valence electrons on s, p and d orbitals;[26] modulations of the numbers of valence electrons by M dopants can stabilize the structure of Sm(Co, M)$_7$.

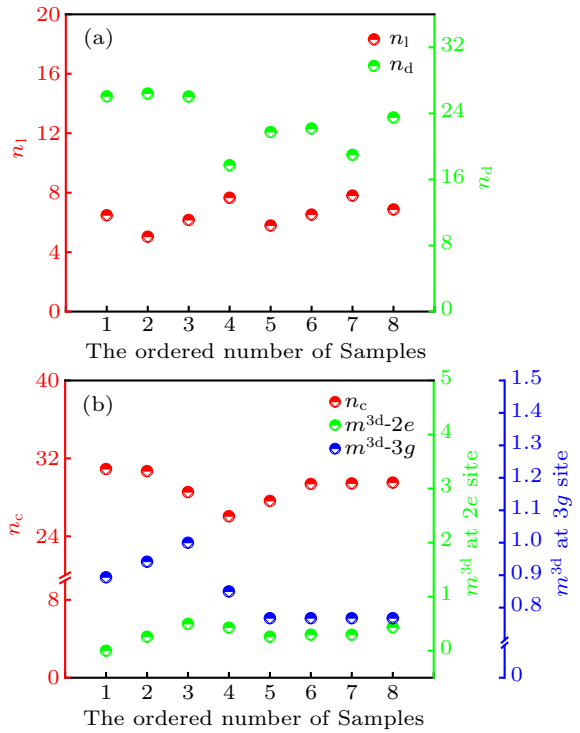


Fig. 3. The distributions of various electrons in Sm(Co, M)$_7$: the numbers of covalence electrons n_c, valence electrons n_d and lattice electrons n_l are shown in (a) and the distribution of covalence electrons n_c and 3d magnetic electrons of Co atoms at 2e and 3g sites are shown in (b). 1, $SmCo_{6.9}Hf_{0.1}$; 2, $SmCo_{6.9}Zr_{0.1}$; 3, $SmCo_{6.1}Si_{0.9}$; 4, $SmCo_6Ga$; 5, $SmCo_{5.7}Ga_{1.3}$; 6, $SmCo_{6.2}Cu_{0.8}$; 7, $SmCo_{5.5}Cu_{1.5}$; 8, $SmCo_4Cu_3$.

3.2. Melting point, cohesive energy and valence electron structure

The calculated melting points are in good agreement with the experimental ones estimated by the weighted average of the liquid phase temperature in the binary phase diagram. The calculated melting points exhibit a positive correlation with the maximum number of covalent electron pairs n_A except for the anomalous $SmCo_{7-x}Cu_x$. With increase in n_A, more vibration energy of thermal phonons is required to break the structural framework, leading to a higher melting point. However, $SmCo_{7-x}Cu_x$ shows a reverse correlation between T_m and n_A. According to the melting point model in Eq. (14), T_m is positively related to n_A, f and b_l, so the decrease of T_m for $SmCo_{7-x}Cu_x$ is due to the anomalous shielding factor b_l of Cu since the b_l of Cu (86.25 kJ·Å/mol) is much lower than those of Co (104.65 kJ·Å/mol) and Sm (191.4329 kJ·Å/mol).

The calculated cohesive energies exhibit excellent consistency with the mixing energies estimated by the sum of the cohesive energy of individual atoms. As shown in Fig. 4(b), the trend of variation of cohesive energies shows a positive relation to the number of covalence electrons n_c. An increase in the number of covalence electrons strengthens the bonding interactions between atoms, thereby increasing the cohesive energy and stabilizing the crystal structure.

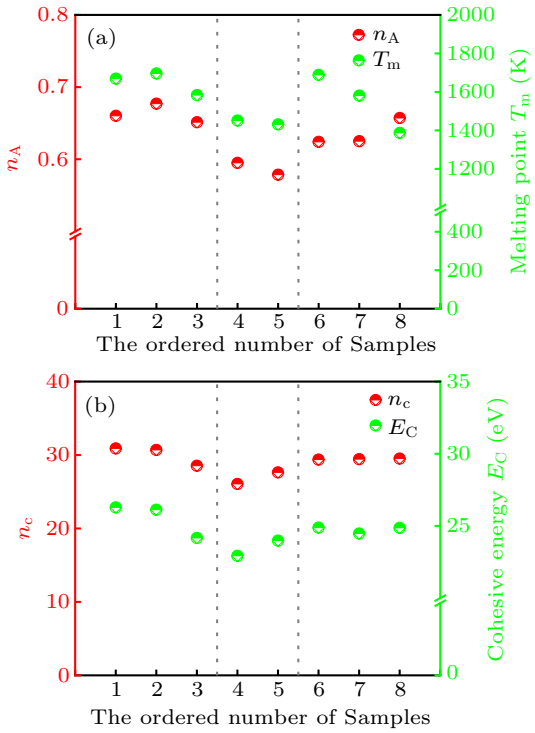


Fig. 4. The strong correlation between physical properties and valence electron structures in Sm(Co, M)$_7$. The melting points and the maximum number of covalent electron pairs n_A are shown in (a) and the cohesive energies and covalence electrons number n_c in (b). 1, $SmCo_{6.9}Hf_{0.1}$; 2, $SmCo_{6.9}Zr_{0.1}$; 3, $SmCo_{6.1}Si_{0.9}$; 4, $SmCo_6Ga$; 5, $SmCo_{5.7}Ga_{1.3}$; 6, $SmCo_{6.2}Cu_{0.8}$; 7, $SmCo_{5.5}Cu_{1.5}$; 8, $SmCo_4Cu_3$.

3.3. Magnetic properties and valence electron structure

The moments calculated by the structural formula unit match the experimental ones well, as listed in Table 1. To reveal the magnetism of Sm(Co, M)$_7$ intermetallic compounds, the three Co sublattice moments are supplied in Table 2; it can be observed that the sublattice moments corresponding to the 2c site range from 1.2856 μ_B to 2.9612 μ_B, to the 3g site from 0.8499 μ_B to 0.9999 μ_B and to the 2e site from 0 to

0.4957 μ_B. Since the moment is positively related to the number of 3d magnetic electrons, the Co sublattice at the 2*c* site predominantly contributes to the magnetic moment due to its greater number of 3d magnetic electrons. The reduction in the number of 3d magnetic electrons in the 2*e* and 3*g* sublattices is attributed to electron transitions from 3d magnetic electrons to covalence electrons, which causes the increase of numbers of covalence electrons and enhances the bonding strengths between Sm and Co/M at the 3*g* site and Co–Co at the 2*e* site, thus stabilizing the crystal structure of Sm(Co, *M*)$_7$.

Table 1. The calculated and experimental magnetic moments ($\bar{M}_s$ and M_s) and Curie temperature ($\bar{T}_c$ and T_c) of Sm(Co, *M*)$_7$.

Compound	$\bar{M}_s$ (μ_B)	M_s (μ_B)	$\frac{\Delta M_s}{M_s}$ (%)	$\bar{T}_c$ (K)	T_c (K)	$\frac{\Delta T_c}{T_c}$ (%)
$SmCo_{6.9}Hf_{0.1}$	8.549	8.32[18]	2.75	1181.92	1080[7]	9.35
$SmCo_{6.9}Zr_{0.1}$	7.850	7.66[16]	2.48	1083.44	1178[15]	8.03
$SmCo_{6.1}Si_{0.9}$	5.046	5.41[37]	6.72	758.95	717[37]	5.85
$SmCo_6Ga$	5.396	4.9[38]	10.12	1148.38	1100[18]	4.36
$SmCo_{5.7}Ga_{1.3}$	4.559	4.9[38]	6.95	1127.76	1085[18]	3.87
$SmCo_{6.2}Cu_{0.8}$	5.851	5.87[17]	0.3	1095.61	1128[17]	2.93
$SmCo_{5.5}Cu_{1.5}$	5.693	5.49[17]	3.6	1052.06	1101[17]	4.45
$SmCo_4Cu_3$	4.557	–	4.3	905.35	–	–

Table 2. Corresponding 3d magnetic electrons and covalence electrons n_c of Co sites in Sm(Co, *M*)$_7$.

Compound	Co site	m^{3d}	n_c
$SmCo_{6.9}Hf_{0.1}$	2*e*	0	7
	2*c*	2.9342	4.0658
	3*g*	0.8936	6.1064
$SmCo_{6.9}Zr_{0.1}$	2*e*	0.2586	6.7414
	2*c*	2.9612	4.0776
	3*g*	0.9416	6.3723
$SmCo_{6.1}Si_{0.9}$	2*e*	0.4957	6.0085
	2*c*	1.2856	5.7144
	3*g*	0.9999	5
$SmCo_6Ga$	2*e*	0.4262	5.7214
	2*c*	1.712	5.288
	3*g*	0.8499	4.4504
$SmCo_{5.7}Ga_{1.3}$	2*e*	0.2586	6.7414
	2*c*	1.4872	6.0085
	3*g*	0.7674	4.6979
$SmCo_{6.2}Cu_{0.8}$	2*e*	0.2953	6.1141
	2*c*	1.9628	5.6915
	3*g*	0.7674	4.6979
$SmCo_{5.5}Cu_{1.5}$	2*e*	0.2953	6.1141
	2*c*	1.8837	5.1163
	3*g*	0.7674	4.6979
$SmCo_4Cu_3$	2*e*	0.4333	6.5667
	2*c*	1.2856	5.7144
	3*g*	0.7674	4.6979

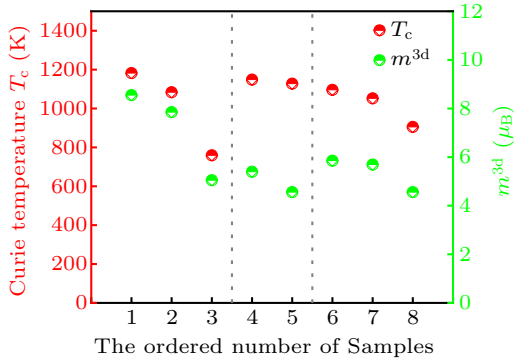


Fig. 5. The strong correlation between Curie temperature and moment in Sm(Co, *M*)$_7$. 1, $SmCo_{6.9}Hf_{0.1}$; 2, $SmCo_{6.9}Zr_{0.1}$; 3, $SmCo_{6.1}Si_{0.9}$; 4, $SmCo_6Ga$; 5, $SmCo_{5.7}Ga_{1.3}$; 6, $SmCo_{6.2}Cu_{0.8}$; 7, $SmCo_{5.5}Cu_{1.5}$; 8, $SmCo_4Cu_3$.

The calculated Curie temperatures are also in good agreement with the experimental ones. As shown in Fig. 5, the trend of change of the total number of 3d magnetic electrons is similar to that of the Curie temperature, indicating that the Curie temperatures are strongly and positively related to the number of 3d magnetic electrons. With increase in the number of 3d magnetic electrons, it is necessary to have more thermal phonons to break the ordered magnetic structure, leading to an increase in the Curie temperature.

4. Conclusion and perspectives

In this study, the relationship between the valence electronic structure, structural stability, melting point and cohesive energy in Sm(Co, *M*)$_7$ intermetallic compounds has been revealed by using an empirical electron theory of solids and molecules (EET). The structural stability is strongly related to the valence electronic structure modulated by doping the third element *M* into $SmCo_7$. The calculated bond length, melting point, magnetic moment and Curie temperature agree well with the experimental ones. The calculated cohesive energy is consistent with the estimated one according to the cohesive energy of each atom, which is proportional to the number of covalence electrons n_c. The melting point is closely correlated with the maximum number of covalent electron pairs n_A, shielding factor b_1 and bonding factor f. The magnetic moment and Curie temperature strongly depend upon the number of 3d magnetic electrons, which can be modulated by mutual electron transformations between 3d magnetic electrons and covalence electrons. Consequently, Sm–Co 1:7 type pseudobinary intermetallic compounds with exceptional magnetic properties and thermal stability can be successfully developed by the optimization of their valence electron structures.

References

[1] Han C Y, Lu H, Xu G J, Li Y R, Liu X M and Song X Y 2024 *Mater. Today Phys.* **40** 101306

[2] Song W P, Li X H, Lou L, Hua Y X, Zhang Q, Huang G W and Zhang X Y 2017 *APL Mater.* **5** 116101
[3] Guo J G, Chen N X and Shen J 2006 *J. Alloys Compd.* **425** 14
[4] Buschow K H J, Fast J F and Goot A S V D 1968 *Phys. Status Solidi B* **29** 825
[5] Guo Z H, Hsieh C C, Chang H W, Zhu M G, Pan W, Li A H, Chang W C and Li W 2010 *J. Appl. Phys.* **107** 09A705
[6] Al-Omari I A, Yeshurun Y, Zhou J and Sellmyer D J 2000 *J. Appl. Phys.* **87** 6710
[7] Luo J, Liang J K, Guo Y Q, Yang L T, Liu F S, Zhang Y, Liu Q L and Rao G H 2004 *Appl. Phys. Lett.* **85** 5299
[8] Luo J, Liang J K, Guo Y Q, Liu Q L, Liu F S, Zhang Y, Yang L T and Rao G H 2004 *Intermetallics* **13** 710
[9] Zhang D T, Yue M, Pan L J, Li Y C, Xu G, Liu W Q, Zhang J X, Liu X B and Altounian Z 2008 *J. Appl. Phys.* **103** 07E124
[10] Feng D Y, Zhao L Z and Liu Z W 2016 *Physica B* **487** 25
[11] Liu Z, Chen R J, Lee D and Yan A R 2011 *J. Alloys Compd.* **509** 3967
[12] Hsieh C C, Shih C W, Liu Z, Chang W C, Chang H W, Sun A C and Shaw C C 2012 *J. Appl. Phys.* **111** 07E306
[13] Hsieh C J, Chang H, Zhao X G, Sun A and Chang W 2011 *J. Appl. Phys.* **109** 07A730
[14] Hsieh C C, Huang S T, Guo J S, Shih C W, Chang W C, Chang H W and Shaw C C 2013 *J. Korean Phys. Soc.* **63** 401
[15] Huang M Q, Wallace W E, McHenry M, Chen Q and Ma B M 1998 *J. Appl. Phys.* **83** 6718
[16] Feng D Y, Liu Z W, Zheng Z G, Zeng D C and Zhang G Q 2013 *J. Magn. Magn. Mater.* **347** 18
[17] Guo Y Q 2006 *J. Baotou Univ. Iron Steel Technol.* **25** 139
[18] Guo Y Q, Feng W C, Li W, Luo J and Liang J K 2007 *J. Appl. Phys.* **101** 023919
[19] Li Y Y, Shen J and Chen Y 2010 *Solid State Sci.* **12** 33
[20] Liu L L and Jiang C B 2012 *J. Supercond. Nov. Magn.* **25** 131
[21] Sabirianov R F, Kashyap A, Skomski R, Jaswal S S and Sellmyer D J 2004 *Appl. Phys. Lett.* **85** 2286
[22] Mao F, Lu H, Liu D, Guo K, Tang F W and Song X Y 2019 *J. Alloys Compd.* **810** 151888
[23] Guo Y Q, Yü R H, Zhang R L, Zhang X H and Tao K 1998 *J. Phys. Chem. B* **102** 9
[24] Wang X Z, Guo Y Q, Li B Y, Feng Y C and Tang W 2025 *Physica E* **165** 116124
[25] Li B Y, Guo Y Q, Yang Z Y, Wang X Z, Feng Y C and Tang W 2024 *Phys. Chem. Chem. Phys.* **26** 25819
[26] Feng Y C, Guo Y Q, Yao Y, Liu W, Li B Y, Wang X Z and Tang W 2025 *Inorg. Chem.* **64** 7753
[27] Li B Y, Guo Y Q, Feng Y C, Wang X Z and Liu W 2024 *Chin. Phys. B* **33** 116102
[28] Wu W X, Xue Z Y, Hong X, Li X M and Guo Y Q 2009 *Sci. China Ser. G* **52** 864
[29] Xue Z Q and Guo Y Q 2016 *Chin. Phys. B* **25** 063101
[30] Meng Z H, Fu L, Mei J and Guo Y Q 2013 *Sci. Sin. Phys. Mech. Astron.* **43** 275
[31] Guo Y Q, Su T, Zhang J, Wang X Q, Chen Y and Zhao X 2020 *ACS Appl. Energy Mater.* **3** 5361
[32] Yang Z Y, Guo Y Q, Zhang X P, Tang W, Li B Y and Feng Y C 2024 *J. Energy Storage* **91** 111963
[33] Guo X P, Guo Y Q and Yin L H 2022 *J. Alloys Compd.* **896** 162892
[34] Yin L H, Guo X P, Guo Y Q, Hui Y Z and Lu S 2023 *J. Alloys Compd.* **965** 171357
[35] Wang T, Guo Y Q and Li S 2017 *Chin. Phys. B* **26** 103101
[36] Feng Y C, Guo Y Q, Yao Y, Liu W, Li B Y, Yin L H and Wang T 2023 *J. Phys. Chem. C* **127** 21328
[37] Luo J, Liang J K, Guo Y Q, Liu Q L, Yang L T and Liu F S 2004 *Appl. Phys. Lett.* **84** 3094
[38] Guo Y Q, Li W and Feng W C 2005 *Appl. Phys. Lett.* **86** 192513